Inelastic Scattering of Electrons by Helium*

R. S. Oberoi and R. K. Nesbet
IBM Research Laboratory, San Jose, California 95114
(Received 16 April 1973)

Bethe-Goldstone continuum equations for the scattering of electrons from helium are solved variationally in the energy range between the $n = 2$ and $n = 3$ thresholds. Polarization and correlation effects are included in the calculations by allowing for virtual excitation of the $2s$ electron. Shape resonances are found above the $2\,^3S$ threshold, in substantial agreement with close-coupling calculations of Burke, Cooper, and Ormonde. Structures observed immediately below the $3\,^3S$ threshold in experimental cross sections for metastable formation are attributed to several Feshbach resonances whose energies and widths are computed. Cross sections are presented for elastic and inelastic scattering involving the ground state and $n = 2$ states of helium. Cusp behavior, expected at various inelastic thresholds and found in the variational calculations, accounts for several prominent structural features in the scattering cross sections. The present computed results are compared with previous theoretical studies and, wherever possible, with experimental data.

I. INTRODUCTION

In this paper, we present the results of variational calculations of the scattering of electrons by helium in the energy range between the $2\,^3S$ and $3\,^3S$ thresholds. Bethe-Goldstone equations describing the virtual excitation of $2s$ electron are solved for s, p, and d partial waves. The present work is an extension of the work of Sinfailam and Nesbet[1] on elastic scattering from the ground state of helium. We confirm the presence of $^2P^o$ and $^2D^e$ shape resonances at roughly the positions predicted by the close-coupling calculation of Burke, Cooper, and Ormonde.[2] Several Feshbach resonances below the $3\,^3S$ threshold are computed for the first time. The evidence for these resonances has been obtained in several experimental measurements.[3-7] These resonances below the $3\,^3S$ threshold have not been found in close-coupling calculations[2] based on the lowest five states of the target atom, namely, the ground state and $n=2$ states of helium. This results from omission of the $n=3$ states from the expansion of the wave function. Furthermore, in solving the close-coupling equations, Burke *et al.*[2] have simplified the contribution from an exchange term by assuming that the target states used in their calculation are exact solutions of the two-electron Schrödinger equation. According to Burke *et al.*,[2] this approximation introduces an error of unknown magnitude in their calculation and is most important for low partial waves. In particular, the s-wave contribution to the cross section for metastable production, in their calculation, had to be divided by 10 to obtain good agreement with the experimental cross section. In spite of this approximation, however, their calculation successfully obtains the shape resonances above the $2\,^3S$ threshold. Sklarew and Callaway[7] have attempted to include polarization and distortion effects in the elastic scattering of electrons from the $2\,^3S$ state of helium by a polarized-orbital-type calculation.

The plan of the rest of the paper is as follows: Sec. II contains a brief discussion of the method used. In Sec. III we describe the basis functions used in the present work. Section IV contains the results of the calculations, which are compared with earlier theoretical work[2,8] and, wherever possible, with experimental results. Our conclusions are summarized in Sec. V.

II. COMPUTATIONAL METHOD

The computational procedure for the variational solution of Bethe-Goldstone equations has been described elsewhere.[1,8] Here we summarize the nature of the wave function used and the procedure used to calculate cross sections. First we shall consider the formalism appropriate to an electron-atom-system wave function which has well-defined values of M_L, M_S, and parity π. The reactance matrix K, corresponding to a wave function which is an eigenfunction of L^2, S^2, and π, can be easily derived.

The $(N+1)$-electron wave function describing the scattering of an electron by an N-electron atom is written

$$\Psi = \sum_p \mathcal{A}\Theta_p\psi_p + \sum_\mu \Phi_\mu c_\mu \,. \tag{1}$$

Here Θ_p is a normalized stationary state of the target atom corresponding to open scattering channel p; ψ_p is the corresponding one-electron open-channel orbital with angular momentum l_p and wave-vector magnitude k_p; Φ_μ is one of the assumed orthonormal set of $(N+1)$-electron Slater

determinants. The operator $\mathcal{A}$ antisymmetrizes $\Theta_p\psi_p$. The quadratically integrable function

$$\Psi_H = \sum_\mu \Phi_\mu c_\mu \tag{2}$$

is the Hilbert-space component of Ψ.

The Slater determinants Φ_μ are obtained from a reference Slater determinant

$$\Phi_0 = \det\phi_1(1)\cdots\phi_N(N) \tag{3}$$

by replacing the occupied orbitals $\phi_i\phi_j,\ldots,$ $(i<j\cdots\leq N)$ with orthonormal unoccupied orbitals $\phi_a\phi_b,\ldots$ and adding an unoccupied orbital $\phi_c (N<a<b\cdots<c)$. Thus, in particular,

$$\Phi_{ij}^{abc} = \det'\phi_1(1)\cdots\phi_a(i)\phi_b(j)\cdots\phi_N(N)\phi_c(N+1) \tag{4}$$

represents a two-electron virtual excitation (ab/ij) coupled to an additional unoccupied orbital ϕ_c. The notation det′ implies antisymmetrization and appropriate normalization. Polarization and correlation effects are thus included through Ψ_H, the Hilbert-space component of the wave function.

The target-atom wave function Θ_p can be expressed in the form

$$\Theta_p = \sum_\sigma \Phi_\sigma c_\sigma^p , \tag{5}$$

where each Φ_σ is a normalized N-electron Slater determinant constructed from the orbital functions $\{\phi_i;\phi_a\}$. The coefficients c_σ^p can be obtained as a normalizable eigenvector of N-electron Hamiltonian matrix $H_{\sigma\sigma'}$, corresponding to energy E_p. If E is the total energy of the system, an open channel k value is defined by

$$\tfrac{1}{2}k_p^2 = E - E_p \tag{6}$$

for energies in Hartree atomic units.

A modified version of the multichannel Kohn variational method called "optimized anomaly-free method"[9] is used to calculate the reactance matrix K, with the wave function Ψ of Eq. (1) which has fixed values of M_L, M_S, and π. In consequence of linearity of the Schrödinger equation, Eq. (1) can be written

$$\Psi = \sum_p c_p \Psi_p , \tag{7}$$

where Ψ_p is an $(N+1)$-electron function in channel p. The component of the wave function in channel p, $\Psi_p^{\vec{L},\vec{S}}$, corresponding to symmetry-adapted wave function $\Psi^{\vec{L},\vec{S}}$ can be written as a linear combination of functions Ψ_p:

$$\Psi_p^{\vec{L},\vec{S}} = \sum_i a_i^p \Psi_p . \tag{8}$$

With these definitions, it is possible to write the K matrix corresponding to a symmetry-adapted wave function for fixed values of L^2, S^2 and π as

$$K_{pq}^{\vec{L},\vec{S}} = \sum_{ij} a_i^{p+} K_{ij} a_j^q , \tag{9}$$

where K_{ij} is the reactance matrix corresponding to the wave function of Eq. (1) with fixed values of M_L, M_S, and π.

Designating the initial state of the atom by quantum numbers n, L, S or collectively by the symbol γ and a final state by quantum numbers n', L', S' or collectively by the symbol γ', the cross section for the transition $\gamma \to \gamma'$ can be written[10]

$$Q_{\gamma\gamma'} = \frac{\pi}{k_\gamma^2} \sum_{\vec{L},\vec{S}} \frac{(2\vec{L}+1)(2\vec{S}+1)}{2(2L+1)(2S+1)} \sum_{ll'\pi} |T_{\gamma i,\gamma' i'}^{\vec{L},\vec{S},\pi}|^2 , \tag{10}$$

where l and l' are the angular momenta of the external electrons associated with the atomic states γ and γ', respectively, and T is the transmission matrix related to the K matrix via

$$T = 2iK/(1-iK) . \tag{11}$$

III. CHOICE OF BASIC FUNCTIONS

In choosing the basis functions used in the present calculations and listed in Table I, we have closely followed the procedures investigated by Sinfailam and Nesbet.[1] The basis set is used both to get a good representation of the target-atom states and to represent the Hilbert-space component of the wave function. A sequence of exponents in geometrical progression for a fixed n is used. The one-electron basis functions for quantum numbers l, m_l, m_s are of the Slater form

$$n_i = N r^{n_i} e^{-\alpha_i r} Y_{lm_l}(\hat{r}) V_{m_s} . \tag{12}$$

Moreover, the parameters in Eq. (12) are chosen in such a way that the maxima of the functions corresponding to different l lie at the same relative distance from the origin. To keep the size of the basis set within computational convenience, we have not added any orbitals with arithmetic sequence of exponents to those listed in Table I. Thus our basis set of functions can be only approximately complete. Furthermore, the achievement

TABLE I. Basis-set parameters. The orbitals are of the Slater form [Eq. (12)] and $\mu = 0.55$.

$l=0$	$n=1;\ \alpha = 2.0,\ 0.5$
	$n=2;\ \alpha = 0.5/\mu,\ 0.5,\ 0.5\mu,\ 0.5\mu^2,\ 0.5\mu^3,\ 0.5\mu^4$
$l=1$	$n=2;\ \alpha = 0.5/\mu,\ 0.5,\ 0.5\mu,\ 0.5\mu^2,\ 0.5\mu^3,\ 0.5\mu^4$
$l=2$	$n=3;\ \alpha = 0.75\mu,\ 0.75,\ 0.75\mu,\ 0.75\mu^2,\ 0.75\mu^3,\ 0.75\mu^4$
$l=3$	$n=4;\ \alpha = 1.0\mu,\ 1.0,\ \mu,\ \mu^2,\ \mu^3$

of a truly complete basis, by monitoring the rate of convergence with respect to additional basis functions, is more difficult for multichannel scattering if the cross sections have a noticeable structure. This is a consequence of the shifts of relative positions of thresholds by the additional functions. From a limited exploration of the basis set functions, we choose a geometric ratio of 0.55. For s-wave scattering, only s and p orbitals are used; for p waves only s, p, and d orbitals; and for d waves the full basis set of Table I is used.

Basis-set orbitals $\{\phi_i; \phi_a\}$ were generated by performing a matrix Hartree-Fock calculation for the $2\,^3S$ state of helium. The target states were then generated by carrying out a configuration-interaction calculation corresponding to Eq. (5). All configurations of the type $1sns$ and $1smp$ ($n \geq 1$ and $m \geq 2$) were included in the calculation. The computed energies (Table II) of the various $n=2$ states and the $3\,^3S$ state are in good agreement with the experimental values.[11] However, the ground-state energy is rather poor: -78.08 eV as compared with the experimental value of -79.01 eV. This is due to the fact that only the minimal correlation needed to obtain good energy values of the excited states is included in the atomic wave function of Eq. (5). Because of the poor value of the computed ground-state energy, the $2\,^3S$ threshold lies at 18.92-eV electron energy instead of the experimental value of 19.82 eV. The energies of other thresholds differ similarly from the experimental values. In spite of these differences, the relative spacing of $n=2$ thresholds computed here are in reasonably good agreement with the experimental values. Therefore if we fix the computed $2\,^3S$ threshold at its experimental value of 19.82 eV and scale the energies of other thresholds with respect to this value, the agreement between the computed thresholds so scaled and the experimental thresholds is quite good. In presenting our results, we have added to the total energy a value of 0.9 eV, the difference between the computed and experimental energies of the $2\,^3S$ threshold. In actual scattering calculations, however, we have not parametrized the target-state energies and have used the unscaled computed energies.

TABLE II. Energies and excitation thresholds (in eV) of different states of He. The entries in the column for computed thresholds are obtained by fixing the $2\,^3S$ threshold at its experimental value.

	Energies		Thresholds	
State	Computed	Experimental	Computed	Experimental
$1\,^1S$	−78.08	−79.01	···	0.0
$2\,^3S$	−59.16	−59.19	19.82	19.82
$2\,^1S$	−58.32	−58.39	20.66	20.62
$2\,^3P$	−57.99	−58.05	20.99	20.96
$2\,^1P$	−57.76	−57.79	21.22	21.22
$3\,^3S$	−56.29	−56.29	22.69	22.72

A better value of the ground-state energy of helium can be obtained by following the above procedures, starting from a closed-shell matrix Hartree-Fock calculation. However, the relative spacing of $n=2$ levels is observed to be poorer.

The wave function of Eq. (1) used here was taken to be an eigenfunction of M_L, M_S, and π. The quantum numbers M_L, M_S were chosen in such a way that the doublet and quartet contribution for a particular partial wave at a given energy could be calculated simultaneously. Using this procedure, the atomic states with different values of quantum numbers m_l and m_s correspond to different spin-polarized channels even when the scattered electron has the same orbital angular momentum l. Thus for a given energy, the number of spin-polarized open channels far exceeds the number of physical open channels. For example, for s-wave scattering corresponding to an incident electron energy above the $2\,^1P$ threshold, there are thirteen spin-polarized open channels, while there are only five physical open channels for doublet scattering and two physical open channels for quartet scattering. The corresponding numbers for p-wave and d-wave scattering are 16, 7, and 3.

IV. RESULTS

A. Shape Resonances

An isolated resonance in multichannel scattering is described for n coupled channels by n solutions $\delta_j(E)$ of the equation[12]

$$E - E_r = \tfrac{1}{2}\Gamma_r \sum_{i=1}^{n} y_i^2 \cot[\delta_i^0(E) - \delta(E)] \,. \tag{13}$$

The index i refers to an eigenchannel and the background eigenphases $\delta_i^0(E)$ are assumed to be slowly varying functions of energy. Here E_r is the position of the resonance and Γ_r is its width. The sum of eigenphases $\sum_j \delta_j(E)$ increases by π rad in passing through a resonance. Further, since a noncrossing rule holds for the tangent of the eigenphases, an eigenphase associated with a particular eigenchannel below the resonance becomes associated with the next higher one above the resonance.

In Fig. 1, we plot the sum of eigenphases for $^2S^e$, $^2P^0$, and $^2D^e$ electron-helium scattering. Throughout this section, k stands for the magnitude of the momentum of the electron relative to the $2\,^3S$ threshold of He. For $^2P^0$ scattering, the sum

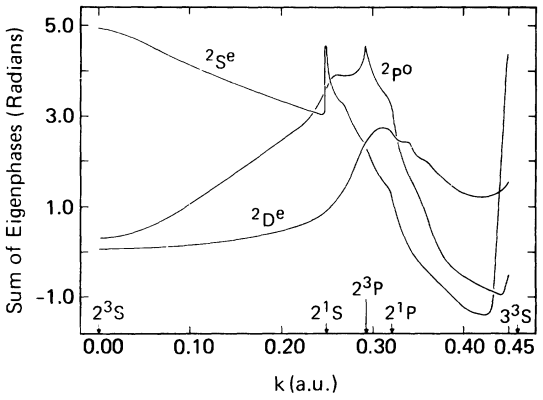

FIG. 1. Sum of eigenphases for $^2S^e$, $^2P^o$, and $^2D^e$ scattering vs k, the magnitude of the electron momentum relative to the $2\,^3S$ threshold.

of the eigenphases starts at approximately 0.32 rad and increases well beyond π rad as k is increased. This is, however, quite a broad resonance, since k has to reach approximately 0.242 before the sum of the eigenphases increases by π rad. The situation with regard to $^2D^e$ scattering is further complicated by the fact that the k interval over which the $^2D^e$ resonance lies is overlapped with new channels opening at the $2\,^1S$, $2\,^3P$, and $2\,^1P$ thresholds of He. The sum of the $^2D^e$ eigenphases increases first slowly, starting from approximately 0.05 rad at the $2\,^3S$ threshold, and then more rapidly past the $2\,^1S$ threshold and reaches a maximum value of 2.67 rad at $k=0.31$. The new eigenphases, at the $2\,^3P$ and 2^1P thresholds, start at π rad and decrease with increasing k, which lowers the sum of eigenphases as k is increased. A similar behavior for the $^2D^e$ eigenphases has been found in the close-coupling calculation of Burke *et al.*[2]

Since these $^2P^o$ and $^2D^e$ resonances are rather broad, and overlapped with new channels, and since background eigenphases are not well determined, the search procedure[13] based on the use of Eq. (13) in the variational method was not successful in correctly predicting their positions. We have, therefore, used the procedure followed by Burke *et al.*,[2] who define the resonance position as the energy where the sum of eigenphases has increased by $\frac{1}{2}\pi$ rad relative to its value at the $2\,^3S$ threshold and determine its width from the slope of the sum of the eigenphases at the resonance position. We find the following parameters for the resonance positions: (i) $^2P^o E_r = 20.17$ eV, $\Gamma_r \approx 0.33$ eV. (ii) $^2D^e E_r = 20.85$ eV, $\Gamma_r \approx 0.20$ eV. Burke *et al.*[2] have estimated $E_r \approx 20.2$ eV, $\Gamma_r \approx 0.4$ eV for the $^2P^o$ resonance and $E_r \approx 21.0$ eV, $\Gamma_r \approx 0.5$ eV for the $^2D^e$ resonance.

These resonances are caused by the dipole-coupling between the $2\,^3S$ and $2\,^3P$ states of He, which are separated by approximately 1.2 eV, and by a similar nondegenerate dipole-coupling between the $2\,^1S$ and $2\,^1P$ states. As expected, no shape resonances were found in s-wave scattering, since the s-wave potential has no centrifugal barrier to support a shape resonance. However, as is clear from Fig. 1, the sum of $^2S^e$ eigenphases rises abruptly for k values slightly above the $2\,^1S$ threshold. This is due to a rapid rise of the $^2S^e$ eigenphase starting at the 2^1S threshold, in agreement with the close-coupling calculation of Burke *et al.*[2] Burke *et al.* reason that this behavior of the $^2S^e$ eigenphase at the $2\,^1S$ threshold indicates a virtual state below the threshold, defined by a pole in the S matrix. The rapid rise of the $^2S^e$ eigenphase sum by nearly 5.7 rad below the $3\,^3S$ threshold is due to the existence of Feshbach resonances and will be considered in Sec. IV B.

Also apparent from Fig. 1 is the discontinuity in the slope of the $^2P^o$ eigenphase sum in passing through the $2\,^3P$ threshold. We also find a similar but less pronounced behavior at the $2\,^1P$ threshold, which is not visible on the scale used in Fig. 1. These structures are consistent with the findings of Bardsley and Nesbet,[14] who studied the threshold behavior of cross sections for the case of long-range potentials. According to Bardsley and Nesbet, a cusp or a point of inflection, associated with infinite slope in the cross sections below and above an excitation threshold, can appear if the scattered electron has zero angular momentum. In the present problem, such structural features can occur at the $2\,^3S$ and $2\,^1S$ thresholds only for s-wave scattering, and at $2\,^3P$ and $2\,^1P$ thresholds only for p-wave scattering.

B. Feshbach Resonances

In contrast with the $n=2$ states, $n=3$ states are more closely spaced. The degeneracy between the $3\,^3S$ and $3\,^3P$ states is broken by a separation of ≈ 0.3 eV, while the energy interval between the $3\,^1S$ and $3\,^3P$ states is ≈ 0.2 eV, and the $3D$ states are effectively degenerate. This situation of $n=3$ states corresponds closely with the corresponding degenerate situation for H. As a result we find several Feshbach resonances below the $3\,^3S$ excitation threshold.

In scanning these Feshbach resonances, we have allowed only the channels corresponding to atomic states $1\,^1S$, $2\,^3S$, and $2\,^1S$ to be open. This is dictated by the relative ease in computations and by the fact that the limited basis of Table I is found to be inadequate when all physical channels are open. A further rationale for this pro-

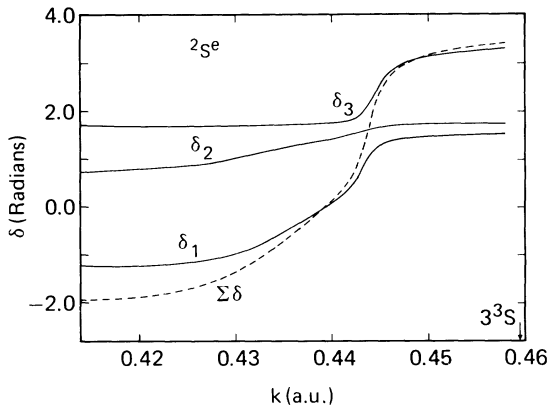

FIG. 2. $^2S^e$ eigenphases and their sum for electron energies near the 3^3S threshold. k is the magnitude of electron momentum relative to the 2^3S threshold.

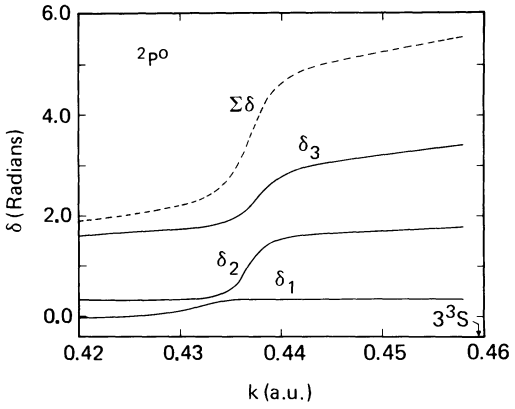

FIG. 3. $^2P^o$ eigenphases and their sum in the vicinity of a Feshbach resonance. k is the magnitude of electron momentum relative to the 2^3S threshold.

cedure is that these resonances are primarily caused by the attractive interaction between the scattered electron and $n=3$ states of He which are well separated from the $n=2$ states. The positions of the resonances, so determined, are not very different from their actual position (when all energetically open channels are included in the computation). This is due to the reason that in our calculations the eigenvalues of the bound-bound matrix responsible for these resonances occur at the same position, irrespective of the number of open channels.

In Fig. 2, we plot the individual eigenphases and their sum (modulo π) for k values below the 3^3S threshold. Here, as in Sec. IV A, k denotes the magnitude of the momentum of the scattered electron relative to the 2^3S threshold. The sum of the eigenphases rises from ≈ -2.0 rad at $k=0.41$ to ≈ 3.4 rad at $k=0.458$, a rise of ≈ 5.4 rad in this k interval. This rise in the sum of eigenphases is 0.9 rad less than the 2π rad. The change in the curvature of the curve for the eigenphase sum and the behavior of the individual eigenphases indicates two $^2S^e$ resonances with different widths. The fact that the sum of the eigenphases rises somewhat less than 2π rad means that these are overlapping resonances, with the tail of the second resonance overlapped with the shoulder of the first. The search procedure[13] confirmed this and produced values of -2.03 and 0.17 rad for the background sum of nonresonating eigenphases, for the two resonances. The widths of these two $^2S^e$ resonances were found to be 0.15 and 0.03 eV, and their positions were found to be 0.28 and 0.19 eV, respectively, below our computed 3^3S threshold. Using the experimental value of 22.72 eV for the 3^3S threshold, we estimate the positions of these resonances to be 22.44 and 22.53 eV.

The individual eigenphases and their sum (modulo π) versus k for a $^2P^o$ resonance are given in Fig. 3. We observe the avoided-crossings of individual eigenphases, characteristic of the multichannel resonances. The sum of eigenphases is seen to rise by approximately π rad in this neighborhood. This $^2P^o$ resonance in our calculation lies 0.27 eV below the 3^3S threshold and for comparison with experiment we estimate its position to be 22.45 eV above the ground state of He. The width is found to be 0.022 eV.

Pichanik and Simpson[3] have observed structural features at electron energies of 22.44 and 22.55 eV in their experimental cross sections for total metastable production, which appear to them to be resonances. These structural features are reproducible to within 0.02 eV in their measurements and they estimate the widths of these resonances to be approximately 0.1 eV. From our calculations it appears that the observed resonances at 22.55 eV is a $^2S^e$ resonance while the observed resonant structure at 22.44 eV is a superposition of $^2S^e$ and $^2P^o$ resonances computed here.

In addition to the doublet resonances, we find a $^4P^o$ Feshbach resonance and evidence of a $^4D^e$ resonance. The individual eigenphases and their sum for the $^4P^o$ resonance are given in Fig. 4. The sum of the eigenphases is found to be increased by π rad in passing through this resonance and the avoided crossings of individual eigenphases are obvious. The search procedure fixed the resonant position at 0.18 eV below the 3^3S threshold, corresponding to a predicted value of 22.54 eV to be compared with experiment. The width of this resonance is found to be 0.05 eV. In computing the $^4P^o$ resonance, all energetically allowed open channels were included. A detailed and exhaustive search did not produce any ^4S resonance. The corresponding calculation for $^4D^e$

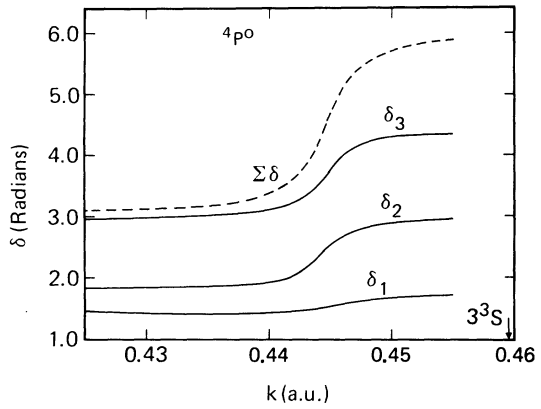

FIG. 4. $^4P^o$ eigenphases and their sum in the vicinity of a Feshbach resonance. k is the magnitude of electron momentum relative to the $2\,^3S$ threshold.

scattering with only a $2\,^3S$ open channel produced a resonance at 22.56 eV having a width of 0.01 eV. To our knowledge, these quartet resonances have not yet been experimentally observed.

C. Cross Sections for Scattering from the Ground State

The scattering of electrons by He in the energy region 19.82 to ≈20.7 eV is characterized by the complex resonant structure due to the resonances described in Secs. IV A and IV B and by the appearance of new channels that open up at the various $n=2$ thresholds. In Fig. 5, we present the cross sections of excitation of the $2\,^3S$ state from the ground state. Also shown are the experimental cross sections measured by Brongersma *et al.*[6] and the results of the five-state close-coupling calculation.[2] Our computed cross sections have the same general features as the measured cross sections but the absolute value of the experimental cross sections are somewhat smaller than our cross sections. This discrepancy may not be very serious since the experimental cross sections have been normalized using the value 4.0×10^{-18} cm^2 (±30%) for the $^2P^o$ resonance peak. In the closecoupling calculations the s-wave contribution to the cross section for $1\,^1S$-$2\,^3S$ transition is larger than resonant p-wave contribution, and to obtain reasonable agreement with the experimental cross sections, only 10% of the s-wave contribution is included in the total cross sections shown in Fig. 5.[2] The s-wave partial cross sections for other excitations, included in total cross sections shown in Figs. 7 and 9, were scaled down in a similar manner.[2] All three sets of results in Fig. 5 show peaks at ≈20.2 and ≈21.0 eV corresponding to the $^2P^o$ and $^2D^e$ shape resonances. The experimental cross sections exhibit another small

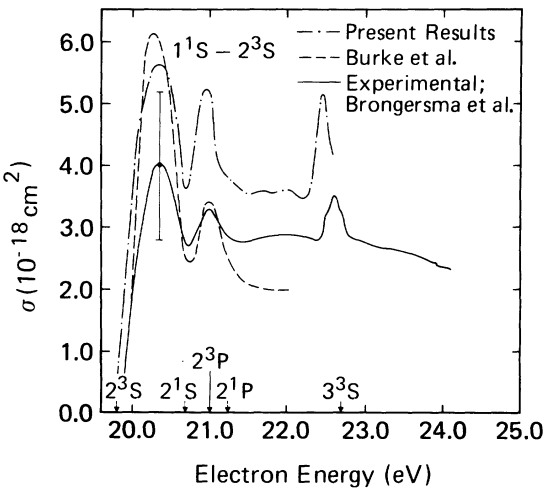

FIG. 5. $1\,^1S$-$2\,^3S$ excitation cross sections. The uncertainty in the absolute value of the experimental cross section at the $^2P^o$ peak is also shown.

but well defined peak at ≈22.6 eV, which is most probably due to the combined effect of several resonances below and above the $3\,^3S$ threshold. The Feshbach resonances below the $3\,^3S$ threshold in our calculation produce a relatively bigger peak at ≈22.45 eV. Figure 6 contains the curves showing the computed spectra for excitation of the $2\,^3S$ state at three different angles of 10°, 30°, and 90°. Our calculations are successful in producing the major features present in the experimental results,[4] viz, the structures associated with the shape resonances and Feshbach resonances.

The cross sections for the $1\,^1S$ -$2\,^1S$ transition are given in Fig. 7. In absolute magnitudes, the experimental cross sections are significantly smaller than the theoretical estimates of the present calculation and those of the close-coupling calculation. Our results show considerable structure between ≈20.6- and ≈22.0- eV electron ener-

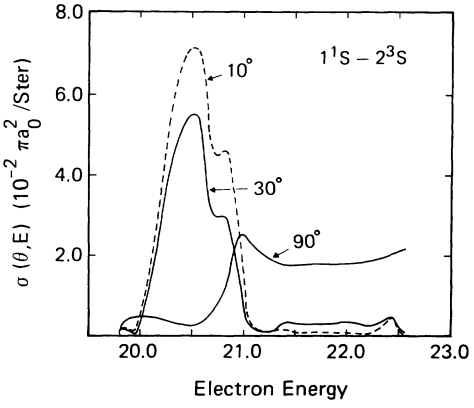

FIG. 6. Spectra for excitation of $2\,^3S$.

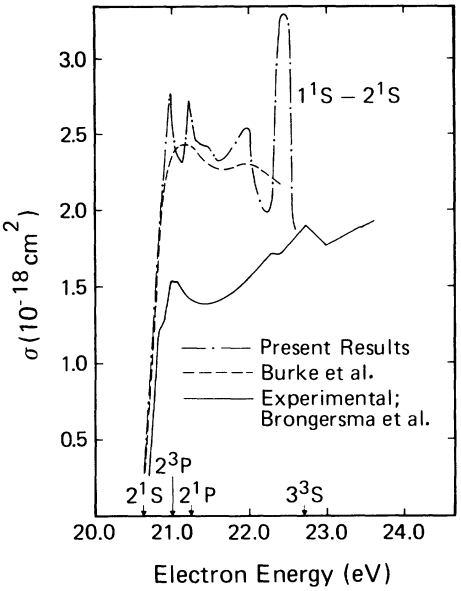

FIG. 7. 1^1S-2^1S excitation cross sections.

gies. The rapid increase in our cross sections up to ≈21.0 eV is due to the contribution from $^2D^e$ resonance, superimposed on a larger contribution from $^2P^o$ scattering which has a cusp at the 2^3P threshold. As stated in Sec. IV A, cusps in the cross sections at the 2^3P and 2^1P excitation thresholds can appear only for p-wave scattering. An example of such a behavior is given in Fig. 8, where we plot, on a fine energy grid, the ^2P cross sections for inelastic scattering from the ground state to the 2^3S and 2^1S states. At the 2^3P threshold, we find a cusp in the cross sections for 1^1S-2^1S excitation and an inverted cusp for 1^1S-2^3S excitation, because in the latter case the slope of the cross sections below the threshold is negative. Another cusp appears in the 1^1S-2^1S excitation cross sections at the 2^1P threshold. The corresponding structure for the 1^1S-2^3S transition is not shown in Fig. 8, since it is much less pronounced and is not well determined in our calculations. Our computed cross sections for the 1^1S-2^1S transition (Fig. 7) also exhibit the resonant structure below the 3^3S threshold. The corresponding structure in the experimental curve is less prominent and once again represents the resonant effects below and above the 3^3S threshold.

The cross sections for excitations of 2^3P and 2^1P states are shown in Fig. 9. Our computed cross sections are in good general agreement with the close-coupling results. As indicated earlier, the cross sections of the close-coupling calculations include only 10% of the contribution from s-wave scattering. If the s-wave partial cross sections were fully included in the close-coupling

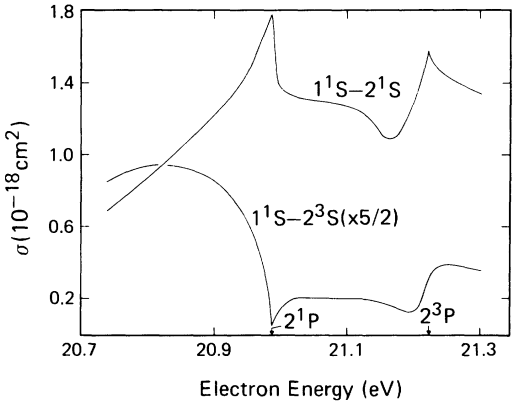

FIG. 8. $^2P^o$ partial-wave cross sections in the neighborhood of 2^3P and 2^1P thresholds.

results, the cross sections for the 1^1S-2^1P transition would be larger than those for the 1^1S-2^3P transition, for electron energies exceeding ≈22.0 eV. Near the 3^3S threshold, the effects of Feshbach resonances are obvious on our cross sections in Fig. 9.

The cross sections for total scattering by the ground state of He are given in Fig. 10. These cross sections decrease with increasing electron energy. However, the total cross sections of our calculation are consistently larger than the experimental cross section[15] by approximately 15%. The corresponding cross sections of the close-coupling calculation are also larger but are closer to the experimental values. A detailed comparison of our cross sections with those of the close-coupling calculation shows that the differences lie primarily in the elastic cross sections; our s-wave and p-wave crosssections being consistently larger. Our elastic crosssections are, however, in better agreement with those of Callaway *et al.*,[16]

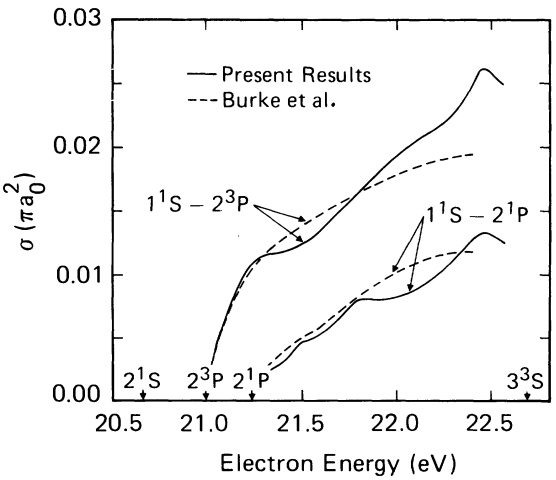

FIG. 9. 1^1S-2^3P and 1^1S-2^1P excitation cross sections.

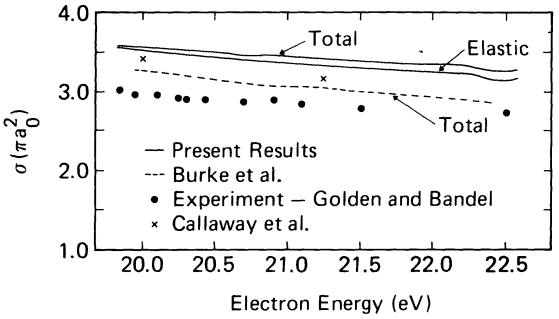

FIG. 10. Elastic and total cross sections for scattering from the ground state.

who have used extended-polarization potential in the polarized orbital method. Their calculations have been performed at only two energies in the energy range considered here and transitions to the $n=2$ levels have not been considered. Our normalization of energy values to the $2\,^3S$ threshold implies that our ground-state elastic-scattering curve is shifted to the right by approximately 1 eV. This can account for a substantial part of the discrepancy in the total cross section. For electron energies below the $2\,^3S$ threshold, results for elastic scattering computed by the present method[1] are in close agreement with polarized orbital calculations and with the experimental cross sections.

D. Cross Sections for Scattering from $n=2$ States

There is a paucity of experimental data for scattering from the $n=2$ states. Neynaber *et al.*[14] have measured total cross sections for scattering from the $2\,^3S$ state at five energies. For the energy region considered here, their measurements are not sufficiently detailed to bring out the resonant structure. We, therefore, compare our results for doublet scattering with the five-state close-coupling[2] calculation and provide our estimates for quartet scattering. The five-state close-coupling calculation has been done only for s-, p-, and d-wave doublet scattering. As in the case of scattering from the ground state, our calculated $^2P^o$ cross sections for scattering from the $n=2$ states show important structural features at the $2\,^3P$ threshold. For example, for elastic-scattering cross sections, we find a cusp for scattering from the $2\,^3S$ state and a point of inflection for scattering from the $2\,^1S$ state. However, these structural features are not obvious in the curves for total cross sections, since, in general, they are masked by the contributions from the $^2D^e$ resonance.

The cross sections for doublet elastic scattering from $2\,^3S$ state are given in Fig. 11. Also shown

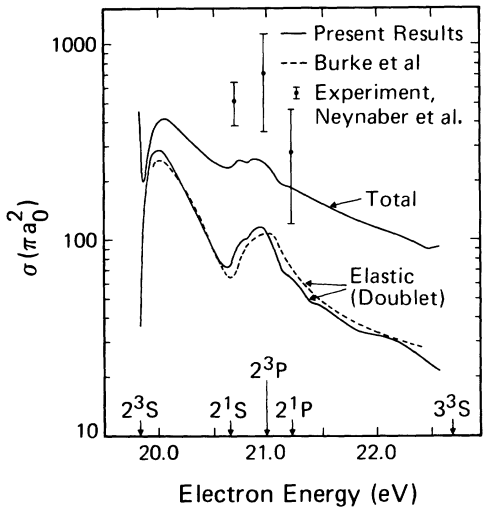

FIG. 11. Elastic and total cross sections for scattering from the $2\,^3S$ state.

are our cross sections for total scattering from this state. Our computed doublet contributions to elastic scattering from $2\,^3S$ state are in reasonably good agreement with those of the close-coupling calculation. Our total cross sections for scattering from this state are, however, smaller than the experimental cross sections,[17] except for one energy. This behavior has been also observed in a close-coupling calculation[2] containing contributions from several higher partial waves. Sklarew and Callaway[7] have performed calculations on the elastic scattering from $2\,^3S$ state, using different approximations of the polarized orbital method. Their cross sections in the adiabatic-exchange approximation are in reasonably good agreement with the experiment, but the extended-polarization approximation cross sections are considerably lower and the resonant structure is not correctly brought out in their computations. The curves for the elastic-scattering cross sections have peaks corresponding to the $^2P^o$ and $^2D^e$ shape resonances. The large value of the total cross section near the $2\,^3S$ threshold is produced by the quartet s-wave elastic scattering which has a scattering length of -33.5 in our computations.

The "virtual state" near the $2\,^1S$ threshold alluded to in Sec. IV A produces large values of cross sections for elastic scattering from the $2\,^1S$ state, shown in Fig. 12. The effect of the $^2D^e$ resonance on these cross sections is a small peak at ≈ 20.9 eV; the corresponding peak in the close-coupling calculation occurs at a slightly larger value of the electron energy. The remaining small structures in our calculations at higher energies probably show that in this energy region our results are not fully converged.

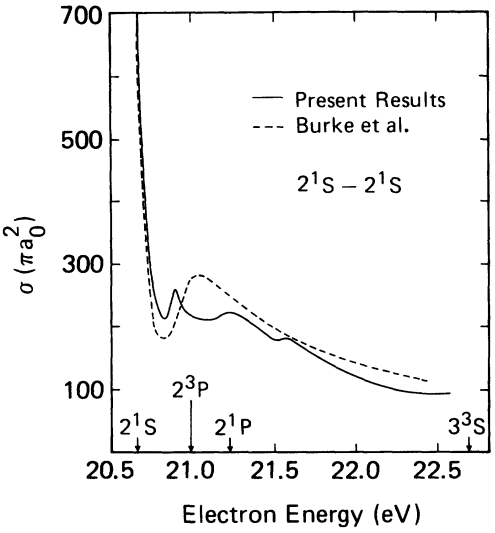

FIG. 12. Cross sections for elastic scattering from the $2\,^1S$ state.

The cross sections for elastic scattering from the $2\,^3P$ and $2\,^1P$ are shown in Fig. 13. The doublet contribution to the $2\,^3P$ elastic-scattering cross sections in our computation are in good agreement with the close-coupling results. For elastic scattering from the $2\,^1P$ state, our cross sections are somewhat smaller than the close-coupling results. However, both sets of calculations show the general feature of decreasing values of cross-sections with increasing electron energy.

The cross sections for excitations from the $2\,^3S$ state are given in Fig. 14. Wherever comparison is possible, our cross sections are in reasonably good agreement with the close-coupling results. The peak in the cross section for $2\,^3S$ -$2\,^1S$ excitation is due to $^2P^o$ resonance and that in the $2\,^3S$ -$2\,^3P$ is due to the $^2D^e$ resonance. The broad peak in the quartet scattering cross sections for the transition $2\,^3S$ -$2\,^3P$ is principally due to the $^4P^o$ resonance below the $3\,^3S$ threshold. The cross sections for inelastic scattering from the $2\,^1S$ and $2\,^3P$ states are given in Fig. 15. The two sets of results for various transitions are in reasonable agreement with each other. For the $2\,^1S$ -$2\,^3P$ transition, our results for ^2P scattering show evidence of a cusp behavior, not explicitly shown in Fig. 15, at the $2\,^1P$ threshold. At higher energies, our computed cross sections for this transition lie around the smooth curve shown in Fig. 15, the largest separation of a computed point from the smooth curve being of the order of 3%. All other curves in Fig. 15 are drawn through actual computed points. This lack of convergence of the cross sections for the $2\,^1S$ -$2\,^3P$ transition

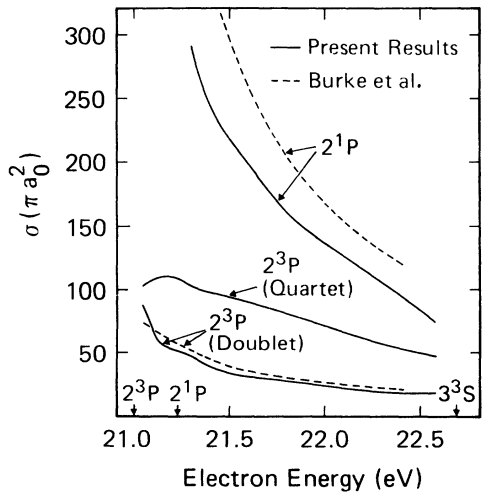

FIG. 13. Cross sections for elastic scattering from the $2\,^3P$ and $2\,^1P$ states.

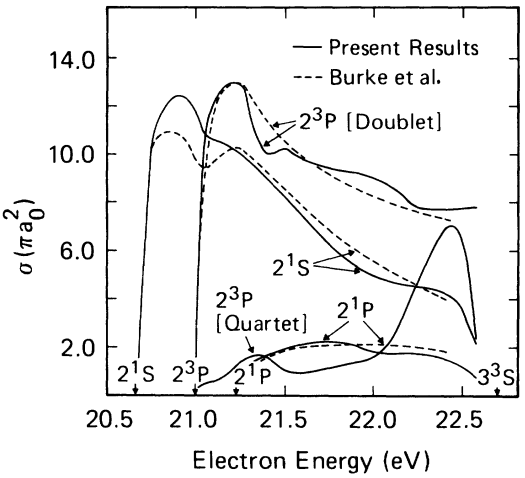

FIG. 14. Cross sections for inelastic scattering from the $2\,^3S$ state.

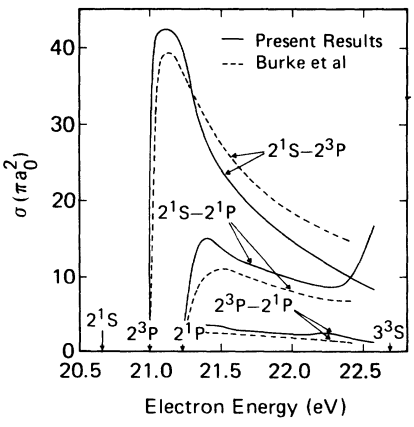

FIG. 15. Cross sections for inelastic scattering from the $2\,^1S$ and $2\,^3P$ states.

and for the elastic scattering from the $2\,^1S$ state (Fig. 12) is not surprising in view of the large dipole polarizability of $2\,^1S$ state which has a value of $802a_0^3$.[18]

V. CONCLUSIONS

We have computed approximate variational solutions of Bethe-Goldstone continuum equations for the scattering of electrons by He in the energy region of excitation of $n=2$ states. By including virtual excitation of the $2s$ electron in our calculations, we have not only included the dominant dipole polarizabilities of the $n=2$ states but also additional contributions to the dynamic energy-dependent response of the target atom to the incident electron.

The calculations reported here have been able to reproduce the $^2P^o$ and $^2D^e$ shape resonance, observed earlier in several experiments[3-6] and found in the close-coupling calculations of Burke *et al.*[2] In absolute magnitudes, our cross sections tend to be somewhat larger than measured values. For example, our computed cross sections for total scattering from the ground state are consistently larger than the experimental cross sections by approximately 15%. This discrepancy is due in part to our definition of energies and k values relative to the $2\,^3S$ threshold, which effectively displaces the $1\,^1S$ elastic cross section by the relative ground-state correlation energy, not computed accurately here. Within the constraints of the basis functions used, our calculations take into account the dynamic response of the target atom to the scattered electron and provide *ab initio* theoretical estimates of the cross sections. The calculations of Burke *et al.*[2] include an approximation for an exchange term. In spite of this approximation, their cross sections for scattering from $n=2$ states are in fairly good agreement with our results and our calculations confirm their contention that the major effect of this approximation is the erroneous nature of their s-wave scattering results for transitions from the ground state to the $n=2$ states.

The principal new theoretical results of the present work concern the computation of energies and widths of two $^2S^e$, one $^2P^o$, one $^4P^o$ and $^4D^e$ Feshbach resonances below the 3^3S threshold. Because of the limited basis used here, we have not been able to obtain convergence in this resonance region. Therefore, except for the $^4P^o$ resonance, the energies and widths of the Feshbach resonances have been determined by excluding the open channels corresponding to the $2\,^3P$ and $2\,^1P$ thresholds. The energies of the Feshbach resonances, so computed, are not expected to be significantly different from their actual positions, since in our calculations the eigenvalues of the bound-bound matrix responsible for the resonances are unaffected by the number of channels allowed to open. The widths, however, are likely to be more dependent upon the approximation used. Evidence for the existence of the doublet resonances has been obtained in several experimental measurements[3-6] and our computed resonance positions are in good agreement with the experimental estimates of Pichanik and Simpson.[3] The quartet Feshbach resonances, predicted by our calculations, have not yet been experimentally observed.

The wave function used here for the electron-atom system has well defined values of M_L, M_S, and parity, but is a superposition of noninteracting LS components. This is due to computational convenience and there is no conceptual problem in calculating physical cross sections associated with an LS wave function. However, this procedure has restricted the size of the basis set that can be used, since the sizes of the matrices that occur in the calculations increase very rapidly as the basis set is enlarged. The sizes of the matrices can be kept reasonable by using a symmetry-adapted wave function and the accuracy of the results can be improved by considering larger basis sets.

The present method is most suitable for investigating resonant phenomenon and other structures in cross sections, such as the cusp behavior here at the $2\,^3P$ and $2\,^1P$ inelastic thresholds. Such structures occur usually in low partial waves. The contributions from higher partial waves, expected to be significant at higher electron energies, can be obtained by using other methods that are computationally simpler.

ACKNOWLEDGMENT

We wish to thank Dr. J. W. Cooper for supplying us with the tabulated cross sections of the five-state close-coupling calculations.

---

*Supported in part by the Office of Naval Research Contract No. N0014-72-0051.

[1] A. L. Sinfailam and R. K. Nesbet, Phys. Rev. A 6, 2118 (1972).

[2] P. G. Burke, J. W. Cooper, and S. Ormonde, Phys. Rev. 183, 245 (1969).

[3] F. M. J. Pichanik and J. A. Simpson, Phys. Rev. 168, 64 (1968).

[4]H. Ehrhardt and K. Willmann, Z. Phys. 203, 1 (1967).
[5]H. Ehrhardt, L. Langhans, and F. Linder, Z. Phys. 214, 179 (1968).
[6]H. H. Brongersma, F. W. E. Knoop, and C. Backx, Chem. Phys. Lett. 13, 16 (1972).
[7]R. C. Sklarew and J. Callaway, Phys. Rev. 153, 81 (1967).
[8]J. D. Lyons, R. K. Nesbet, C. C. Rankin, and A. C. Yates, J. Comput. Phys. (to be published).
[9]R. K. Nesbet and R. S. Oberoi, Phys. Rev. A 6, 1855 (1972).
[10]F. E. Harris and H. H. Michels, Methods Comput. Phys. 10, 143 (1971).
[11]C. E. Moore, *Atomic Energy Levels*, Natl. Bur. Std. Cir. No. 467 (U. S. GPO, Washington, D.C., 1949), Vol. 1.
[12]J. Macek, Phys. Rev. A 2, 1101 (1970).
[13]R. K. Nesbet and J. D. Lyons, Phys. Rev. A 4, 1812 (1971).
[14]J. N. Bardsley and R. K. Nesbet, Phys. Rev. A 8, 203 (1973).
[15]D. E. Golden and H. W. Bandel, Phys. Rev. 138, A14 (1965).
[16]J. Callaway, R. W. LaBahn, R. T. Pu, and W. M. Duxler, Phys. Rev. 168, 12 (1968); R. W. LaBahn and J. Callaway, Phys. Rev. A 2, 366 (1970).
[17]R. H. Neynaber, S. M. Trujillo, L. L. Morino, and E. W. Rothe, *Atomic Collision Processes*, edited by M. R. C. McDowell (North-Holland, Amsterdam, 1964).
[18]K. T. Chung and R. P. Hurst, Phys. Rev. 152, 35 (1966).